Assiut University Journal of Multidisciplinary Scientific Research (AUNJMSR)
Faculty of Science, Assiut University, Assiut, Egypt.
Printed ISSN: 2812-5029
Online ISSN: 2812-5037
The 7th Conference for Young Scientists in Basic and Applied Sciences, May 10 – 11th(2022), Faculty of Science – Assiut University
https://aunj.journals.ekb.eg/

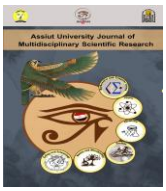

Studies on the structural and optical properties of As_xSe_{100-x} thin films

D. M. Hashem[1,*], A. A. Abu-Sehly[1] , A. A. Joraid[2] , A. Abu El-Fadl[1] and M. M. Hafez[1]

1; Physics Department, Faculty of Science, Assiut University, 71516 Assiut, Egypt.
2; Physics Department, Faculty of Science, Teba University, Saudi Arabia.
*Corresponding Author: i.amunique@hotmail.com

ARTICLE INFO
Article History:
Received: 2022-06-07
Accepted: 2022-06-22
Online: 2022-08-14

Keywords:
Arsenic selenide
Chalcogenide glasses
Optical gap
Oscillator energy

ABSTRACT

Through this paper we discussed some theoretical aspects related to the change in arsinic content in the compound As_xSe_{100-x} . We also presented a discussion on the XRD and optical analyses of the investigated system. The XRD analysis of As_xSe_{100-x} ($5 \leq x \leq 50$) compositions emphases the non crystalline structure of the prepared alloys as well as the evaporated thin films. In the present compound of As_xSe_{100-x}, the rigidity percolation threshold (RPT) occurs at As=40 at.%. Optical investigations of the evaporated As-Se films were done using the recorded data of transmittance (T) and reflectance (R) in the range 350–2500 nm. The optical band gap showed indirect allowed transition for all AsSe thin films of thickness 850 nm. The trend of optical gap of the deposited As_xSe_{100-x} films was found to decrease with increasing of As concentration (upto 40 at.%) and this behavior is explained using two models: Mott and Davis model and the chemical-bond approach (CBA). The dielectric constant at high frequency and the ratios of the carrier concentration to the effective mass were also calculated for the evaporated films. The dispersion behavior of refractive index within the AsSe films was characterized by calculating different parameters such as N/m^*, ε_1, E_o and E_d which were discussed based on the single-oscillator model.

INTRODUCTION

Chalcogenide glasses is one of the most important materials in manufacturing devices. The physical properties of these materials are very interesting, such as high

transmission in the infrared spectrum, elevated refractive index, and reversible non-crystalline to crystalline changes and can be smoothly shaped into optoelectronic devices [1-6]. Among them, the As_xSe_{100-x} ($5 \leq x \leq 50$) glasses are highly recommended materials. Its intrinsic semiconducting manner over a wide band gap as well as interesting switching and photo-darkening characteristics. All these properties make As Se glasses favorable to various technological applications [7,8]. In particular, the Chalcogenide glass $As_{40}Se_{60}$ is very suitable material for all-optical switching devices [9], or as a mid-infrared laser source [10]. Also can be used in optic fibers technology [11]. Moreover, recent studies indicated the possibility to prepare these glasses using different techniques other than the melt-quenching method such as microwave heating [12].

The As Se thin films are also of great interest and have been intensively studied. These studies were derived by their excellent glass forming tendency (up to 40 at% of arsenic), good quality thin films, and their photo- and thermo-induced changes of structure, optical properties, etc. [13]. The tendency of exploration of AsSe thin layers is due to their significant physical properties. In addition to, they are used in the devices of optoelectronics and many optical photonic circuits and their parts (waveguides, gratings, etc.) [13]. Therefore, the optical properties of AsSe should be studied extensively. Thus, lots of work have been made in this paper to study the structural and optical properties of the AsSe chalcogenide materials.

MATERIALS AND METHODS

The bulk alloys of As_xSe_{100-x}, (x = 5, 10, 15, 20, 25, 30, 35, 40, 45, and 50 at. %) were prepared from a mixture of As (purity 99.99%) and Se (purity 99.98%) elements , which were bought from Aldrich Chem. Co., USA by melt-quenching technique. Each element is weighed according to its atomic-weight percentage within the composition, utilizing electronic balance type (Sartorius) with accuracy of $\pm 10^{-1}$ mg, and sealed in silica tubes of 1 cm diameter under vacuum of 5×10^{-5} Torr. The closed tubes heated gradually in an electrical oven up to 850 $^{\circ}$C for 24 hours. The melt was continuously stirred to guarantee better homogeneity. Quenching process was done by immersing the tubes in ice-cold water. Then, the product was taken off the tubes and maintained in a dry atmosphere.

Thin layers of As_xSe_{100-x} ($5 \leq x \leq 50$) were evaporated onto glass substrates at T =27 ^{0}C by the technology of resistive thermal evaporation utilizing a high vacuum coating set up (model: Edward E 306A, UK). The deposited thin layers were of thickness 850 nm.

X-ray diffractometer (PW 1710, Philips Co.) with CuK_α radiation of λ =0.15418 nm and Ni as a filter was used to take X-ray diffraction charts. The diffractometer was conducted at 40 KV and 30 mA. The patterns were measured automatically with a speed of scan of 3.6 deg. min^{-1} and angular of scan (2θ) (4º to 60º).

The optical events such as transmission *(T)*, and reflection *(R)* of the evaporated layers were recorded at T =27 ^{0}C and atmospheric pressure with non-polarized light in the scope of (λ=300-2500 nm) utilizing a scanning spectrophotometer of a double beam (UV-Vis) (model: SHIMADZU UV-2100) united to a computer.

RESULTS AND DISCUSSION

1. Structural analysis of the As-Se compound

Figure. 1 reveals the X-ray diffracted charts of the quenched As_xSe_{100-x} compositions ranging from (***x*** =5-50 at. %) in the bulk form. The patterns revealed amorphous structure for the prepared glasses with two main diffraction humps. Fig. 2 reveals the X-ray diffracted charts of the evaporated As_xSe_{100-x} thin films at room temperature. We couldn't identify any peaks indicating the non crystalline structure of the prepared films.

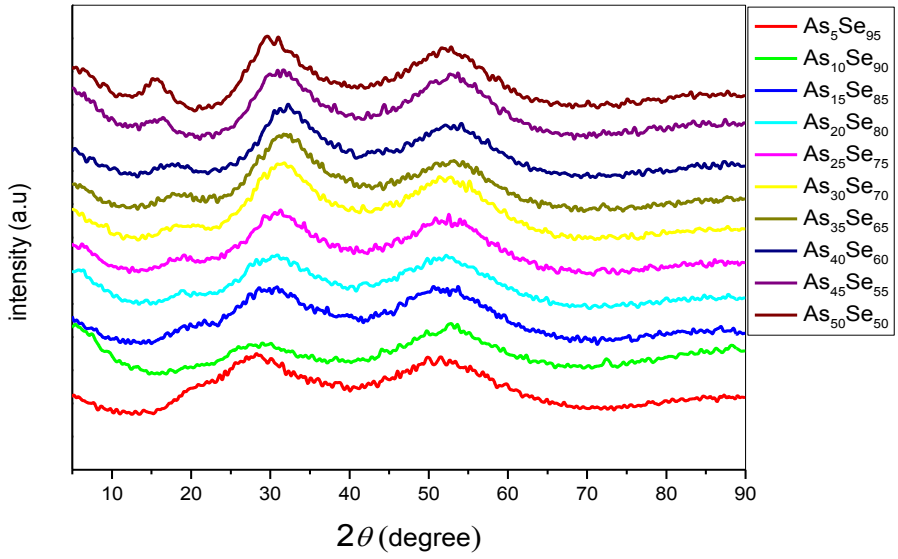

Figure 1: The XRD patterns for As_xSe_{100-x} alloys.

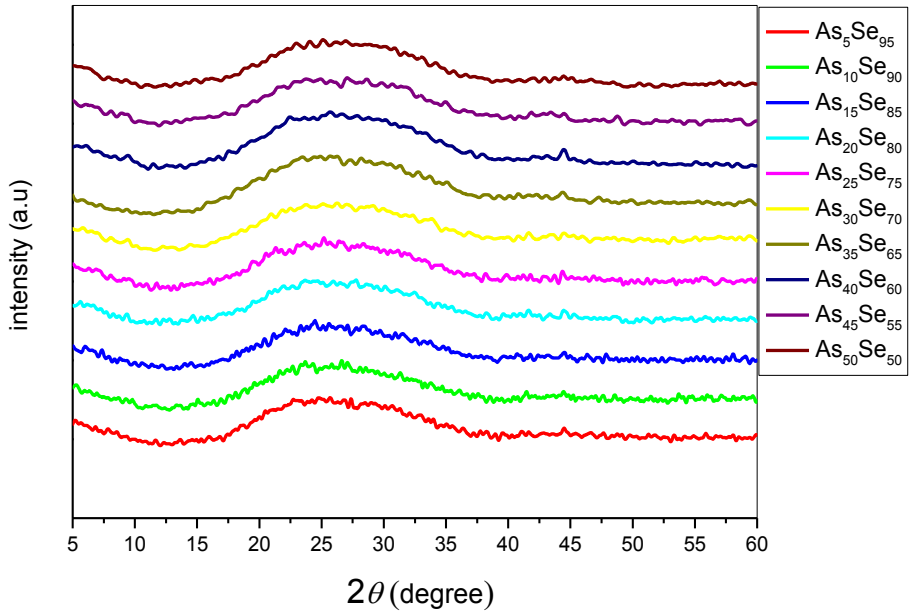

Figure 2: The XRD patterns for As_xSe_{100-x} thin films.

1.1. Structural parameters of AsSe glassy alloys

Preparation of chalcogenide glasses depends on experimental circumstances as the atomic ratio of the used elements, quenching rate, heating program etc. Nonetheless, there are some parameters can give us a previous insight either the target material can be prepared in glass form or not. Parameters such as the average coordination number $\langle r \rangle$, overall mean bond energy $\langle E \rangle$ and average cohesive energy (CE). For binary compounds As_xSe_{100-x} the average coordination numbers $\langle r \rangle$, the total constraints number (N_{con}), the floppy modes fraction f, and deviation of stoichiometry S can be expressed as [14-17]:

$$\langle r \rangle = (xN^{As} + (100 - x)N^{Se})/100 \quad (1)$$

$$N_{con} = \left(\frac{5}{2}\langle r \rangle - 3\right) \quad (2)$$

$$f = \left(2 - \frac{5}{6}\langle r \rangle\right) \quad (3)$$

$$s = \frac{(100 - x)N^{Se}}{xN^{As}} \quad (4)$$

Where N_{As} and N_{Se} are the coordination numbers of *arsenic* and *selenium*, respectively, as listed in Table 1. The calculated values of $\langle r \rangle$, N_{con}, f, and, S are presented in Table 2.

Table1: Physical properties of the constituent elements [18]

Property	**As**	**Se**
Atomic number	33	34
Atomic weight (a.m.u)	74.92	78.96
Density g/cm^3	5.7	4.79
Melting point (K)	814	217
Coordination number (N^X)	3	2
Electronegativity (χ)	2.18	2.55
Bond Energy (Kcal. mol^{-1})	32.1	44.04

Table 2: Physical parameters of As_xSe_{100-x} systems.

Physical parameters	**5**	**10**	**15**	**20**	**25**	**٣٠**	**35**	**٤٠**	**٤٥**	**٥٠**
$\langle r \rangle$	2.05	2.1	2.15	2.2	2.25	2.3	2.35	2.4	2.45	2.5
N_α	1.025	1.05	1.07	1.1	1.12	1.15	1.17	1.2	1.22	1.25
N_β	1.1	1.2	1.3	1.4	1.5	1.6	1.7	1.8	1.9	2
N_{con}	2.12	2.25	2.375	2.5	2.62	2.75	2.87	3	3.12	3.25
S	١٢.٦	٦	٣.٧	٢.٦	٢	١.٥٥	١.٢	١	٠.٨١	٠.٦٦
f	0.29	0.25	0.20	0.16	0.12	0.08	0.04	0	-0.04	-0.08
CE (Kcal. mol^{-1})	44.7	45.5	46.2	47	47.7	48.5	49.2	50.02	49.87	49.71
$\langle E \rangle$ (Kcal. mol^{-1})	79.1	75	70.8	66.6	62.5	58.3	54.1	50.01	56.28	62.53

According to Eq. (1-4). From the constraints theory [14, 15], the value $\langle r \rangle$=2.4 is called the rigidity percolation threshold (RPT). At $\langle r \rangle$ = 2.4, constraints number N_{con} working on the network are counterbalanced by the freedom degree N_d obtainable for the atoms in the network. Thorpe [19] proposed that at this value the glass structure turns into a rigid type instead of an elastically floppy type [20]. in the present system this value is realized for the composition $As_{40}Se_{60}$. Compositions containing As $\leq$ 40, are easy to be prepared in glassy form. Above this value the glass formation becomes more difficult as the structure

becomes more rigid. Added to that decreasing the fraction of floppy modes, f, with increasing As ratio reaching zero at As=40 at.%. This means that the compound becomes more and more rigid with As expansion. Moreover, values of S for the As_xSe_{100-x} ($x < 40$) glasses were > 1 indicating chalcogen-rich compositions and < 1 for compositions with x > 40 indicating chalcogen-poor ones.

1.2 Bond distribution, bond energy, cohesive energy *CE* and overall mean bond energy

The chemical-bond approach (CBA) suggested by Bicerano and Ovshinsky [21] is a reliable method to calculate the predicted bond distribution at different As-Se alloys . The heteronuclear bonds energies (E_{A-B}) were calculated using Pauling's relation [22 ,23]:

$$E_{A-B} = [E_{A-A} \cdot E_{B-B}]^{0.5} + 30(\chi_A - \chi_B)^2 \quad (5)$$

Where E_{A-A} and E_{B-B} are the homonuclear bonds energies in Kcal./ mol. unit, χ_A and χ_B are the electronegativties of the constituent elements A and B respectively. The numerical estimations of the homonuclear bonds and the electronegativity [18] for the arsenic and selenium are shown in Table 1. The expected bonds to form in the As-Se compound are Se-Se (44.04 Kcal./ mol.), As-Se (41.68 Kcal.mol^{-1}), and As-As (32.1 Kcal./mol.).

The cohesive energy (CE) is defined as the energy of stabilization of an infinitely large cluster of the material per atom, which can be calculated using the values of the bonds energies of different bonds involved in the As_xSe_{100-x} (x=5-55 at. %) system. The CE of the as-quenched glassy alloys is estimated from the next relation [24]:

$$CE = \sum Ci\ Di\ /100 \quad (6)$$

Here Ci and Di denote to the number of expected bonds and the corresponding bond energy, respectively. We can notice that the *cohesive energy* increases with increasing the As content up to 40 at.% and decrease for higher Arsenic content, as illustrated in Table ٢. Estimations of the overall mean bond energy $\langle E \rangle$ of the AsSe glasses were calculated by [25]:

$$\langle E \rangle = E_c + E_{rm} \quad (7)$$

where E_c is the overall contribution towards bond energy introduced by strong

heteronuclear bonds [26]. The second term in Eq. (7), E_{rm}, is the contribution arising from weak bonds which remain after all strong bonds have been satisfied [27]. The evaluated numbers are listed in Table ٢.

2. Optical results

2.1. Optical constants of arsenic selenium films

Variation of reflection and transmission of the As_xSe_{100-x} ($5 \leq x \leq 50$) thin layers in the scope of (350–2500) nm is presented in Figs. 3a. From Fig, 3a, we observed distinct interference fringes. The transmission spectra reveal large intensity approaching 83% at longer wavelengths. The intensity of the observed fringes starts to decrease gradually as the absorption event starts to occur within the film until it approaches zero at the edge of the band gap of the evaporated films. Additionally, the transmission spectra show a clear shift to the longer wavelengths as the As concentration increases from (5 to 40 at. %) and blue shift for compositions containing As > 40 at. %. Such changes refer to the compositional dependence of the band gap of the deposited films. A graphical representation of the envelope method is illustrated in Fig. 3b.

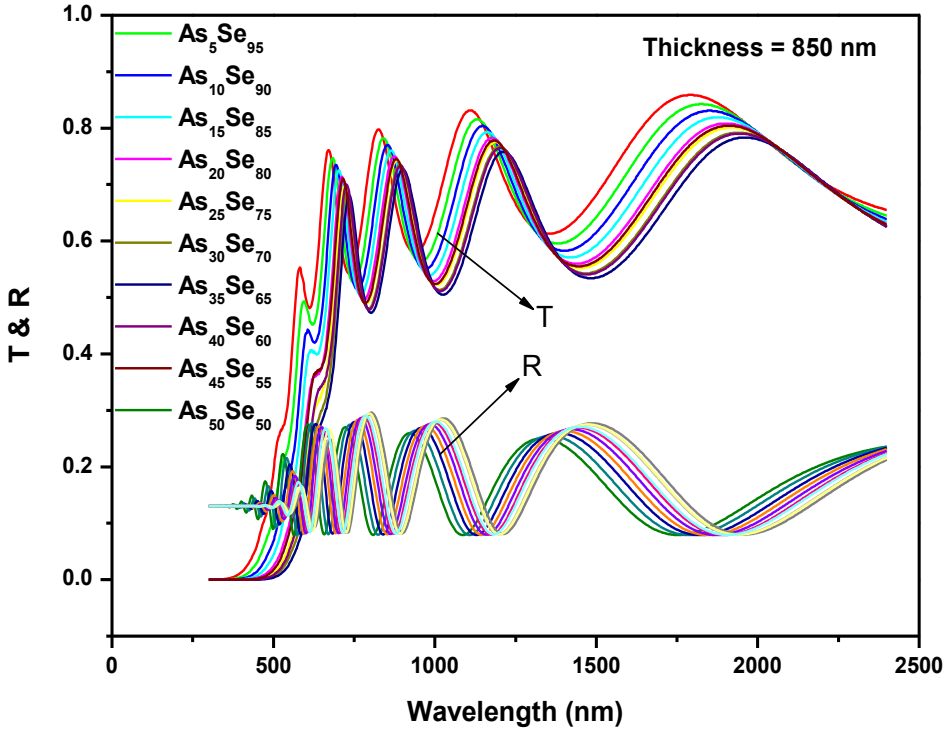

Figure 3a: The spectral distribution of *T* and *R* for As_xSe_{100-x} thin films.

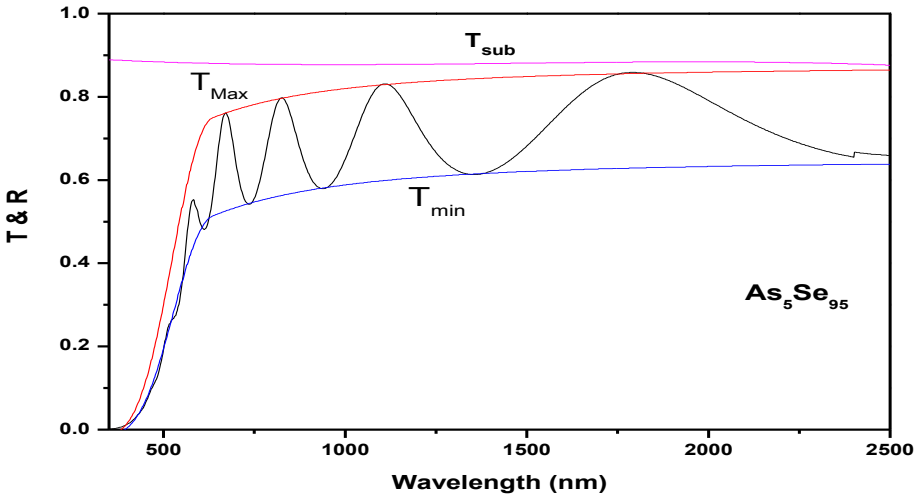

Figure 3b :A graphical representation of the envelope method

Swanepoel [28-30] has stated that the refractive index of the amorphous films can be obtained utilizing an envelope method. The spectral trend of the *n* is obtained from the transmittance spectra of the deposited films in the non-strong absorption areas as shown in Fig. 4. The spectra of *n* may be fitted to the entire wavelength range using different dispersion relations such as, $n = A + B/\lambda^2$ (Cauchy relation). Additionally, Fig. 4 shows decreasing of the refractive index with increasing wavelength. Moreover, it is obvious from Figure 4 that *n* increases gradually with raising As concentration until it approaches its highest value at As=40 at.% and then *n* decreases for compositions containing As>40 at.%.

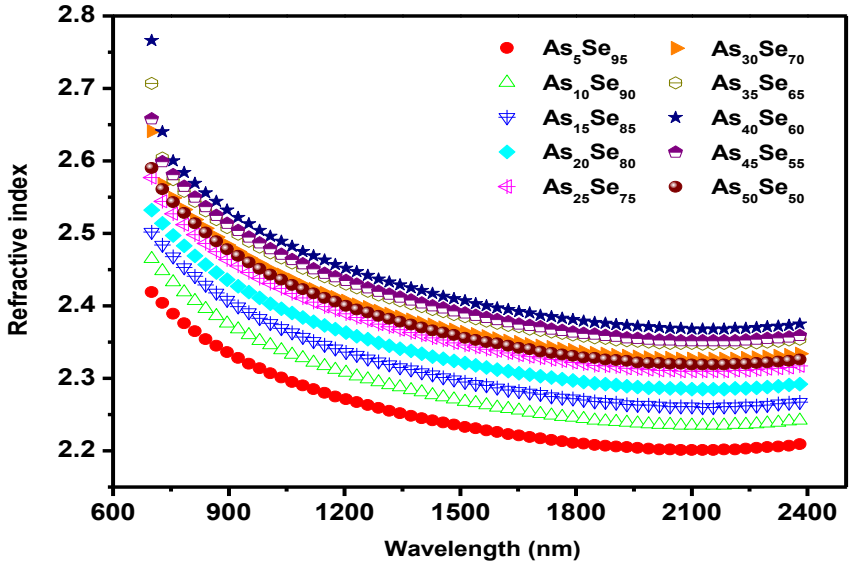

Figure 4: The change of refractive index with wavelength for As_xSe_{100-x} films.

2.2. Single oscillator calculations

In higher wavelengths (normal dispersion in IR region) and according to Drude-Lorentz model, the real part of the complex dielectric constant ε_l is related to λ as fellows [31, 32]:

$$n^2 = \varepsilon_l - Ne^2 / 4\pi^2 c^2 \varepsilon_0 m^*(\lambda^2), \quad (8)$$

where ε_l is the lattice high frequency dielectric constants, e the charge of electron, c the light velocity, ε_o the free space dielectric constant, N/m^* the ratio of free carrier concentration N and m^* is the effective mass.

The plots of n^2 vs. λ^2 is illustrated in Figure 5 for evaporated As_xSe_{100-x} films. Using Eq. (8), the intercept and slope of the linear fits of these plots were used to yield the ε_l and N/m^* ratio values, respectively.

In the transparent region, the n dispersion behavior may be understood on the bases of the single effective oscillator model [33, 34], as described by the next relation:

$$n^2 = 1 + \left(\frac{E_o E_d}{E_o^2 - E^2} \right) \quad (9)$$

where E_o and E_d symbolize the energy of single oscillator and energy of dispersion, respectively. Plotting $1/(n^2 - 1)$ vs. $(E)^2$ (Figure 6) yields straight fitting lines with slope *of* $1/(E_oE_d)$ and intercept of E_o/E_d , which allow us to figure out the E_0 and E_d values. The static dielectric constant **(ε_∞)** was calculated by means of $\left(1 + \frac{E_d}{E_0}\right)$. The energy of oscillator E_o considers as an average energy gap, it changes proportionally with the optical band gap as $E_g \approx E_o/2$.

Another dispersion relation was proposed by Sellmeier [35] to describe the refractive index relationship to the wavelength:

$$n^2 - 1 = \frac{S_o \lambda_o^{\,2}}{1 - \lambda_o^{\,2} / \lambda^2} \quad (10)$$

where S_o and λ_o are the average oscillator strength and wavelength, respectively. The parameters λ_o and S_o were obtained from $(n^2 - 1)^{-1}$ vs. $1/\lambda^2$ spectra (Figure 7). The extracted values from Eqs. (8-10) are listed in Table 3. Figure 8 represents the variation

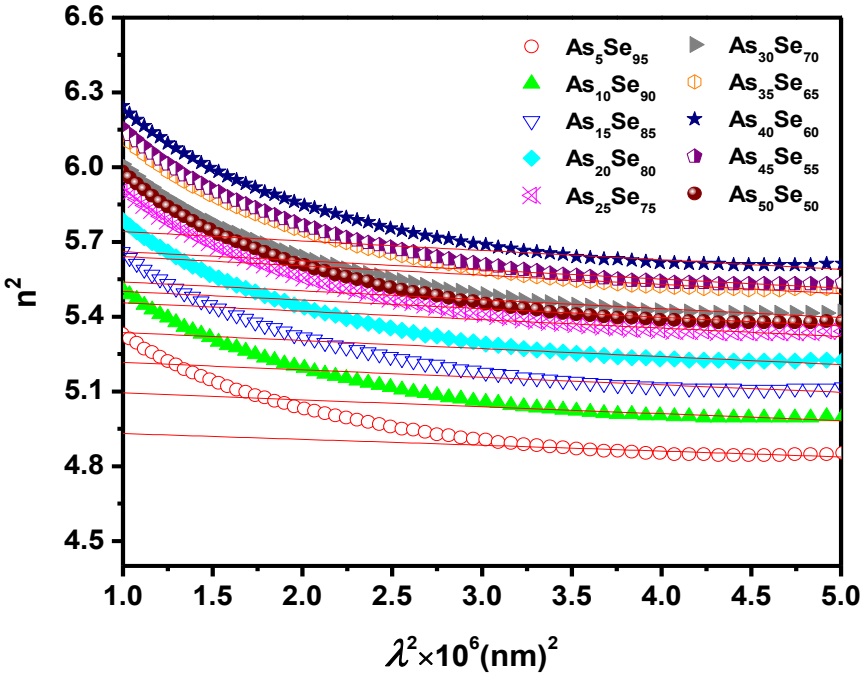

Figure 5: n^2 vs. λ^2 for As_xSe_{100-x} thin films

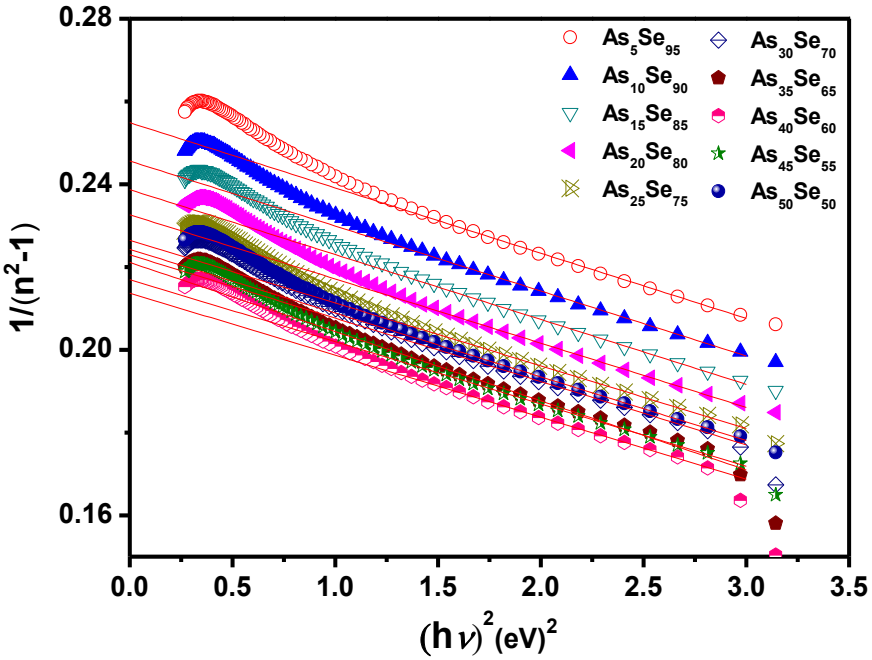

Figure 6: $(n^2-1)^{-1}$ vs. $(h\nu)^2$ for As_xSe_{100-x} thin films

E_o as a function of arsenic concentration. We noticed a decrease in E_0 values with increasing in arsenic content up to 40 at.%. The parameter E_0 is associated to the average molar bond energy of the various involved bonds in the compound [36]. Thus, this

behavior is ascribed to replacing the Se atoms with As atoms, that leads to increasing the number of As-Se weaker bond (41.68 Kcal. mol^{-1}) at the expanse of the basic matrix bonds of Se-Se (44.04 Kcal/mol). Following the graphical representation in Fig. 8, at As>40%, the numbers of E_0 increase with raising As content.

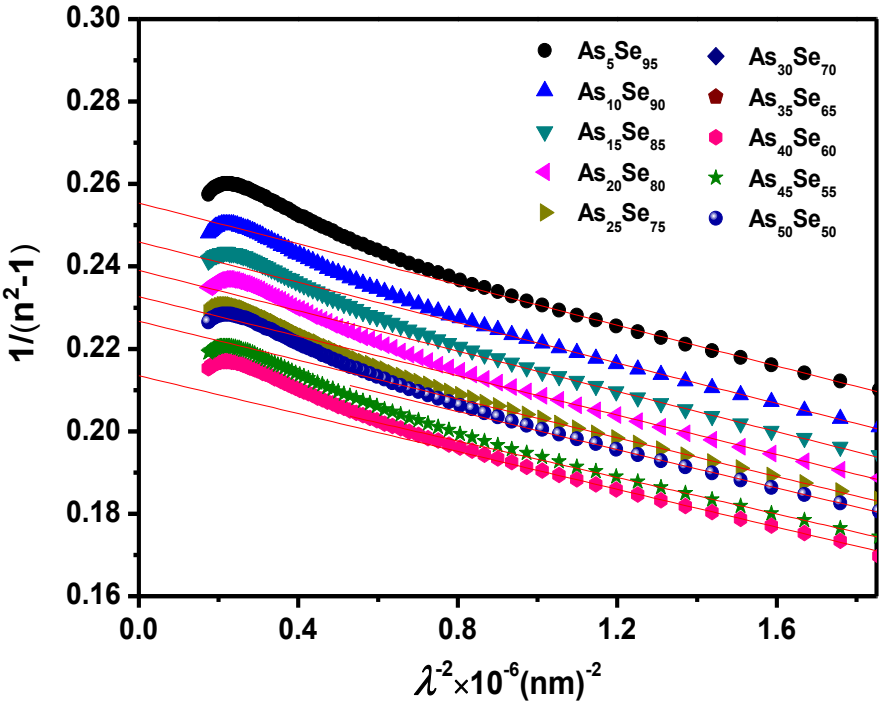

Figure 7: $(n^2-1)^{-1}$ vs. λ^{-2} for As_xSe_{100-x} thin films

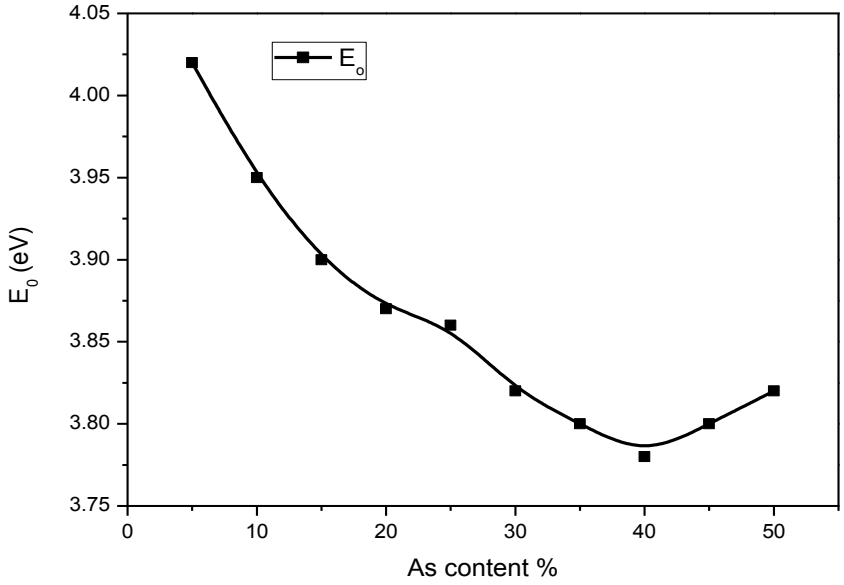

Figure 8: Relation between the single oscillator energy and As concentration

2.3. Calculation of the absorption coefficient, band gap, and extinction coefficient

Figuring out the refractive indices values from the Cauchy relation [37], we can calculate the absorbance $A(\lambda)$ from the interference-free transmission spectra, using the an equation presented by Connell et al. [38]:

$$A = \frac{p + [P^2 + 2QT_\alpha(1 - R_2R_3)]^{1/2}}{Q} \qquad (11)$$

where P=(R_1-1) (R_2-1) (R_3-1), Q=2T_α(R_1R_2+ R_1R_3- 2$R_1R_2R_3$), R_1 is the air-film interface reflectance (R_1=[(1-n)/(1+n)]^2), R_2 is the film-substrate interface reflectance (R_2=[(n-s)/(n+s)]^2), R_3 is the substrate-air interface reflectance (R_2=[(s-1)/(s+1)]^2) ,and T_α is the geometric mean of T_M and T_m [28], T_α=(T_M T_m)$^{0.5}$. knowing the film thickness d , the values of α may be derived by solving the relation $A = exp(-\alpha d)$.

Extinction coefficient is described by $k_{ex}=\alpha\lambda/4\pi$ and employing the values of α and λ we calculate the values of k. Figure 9 shows the relation between α and photon energy, while Figure 10 shows relation between k and wavelength for As_xSe_{100-x} films.

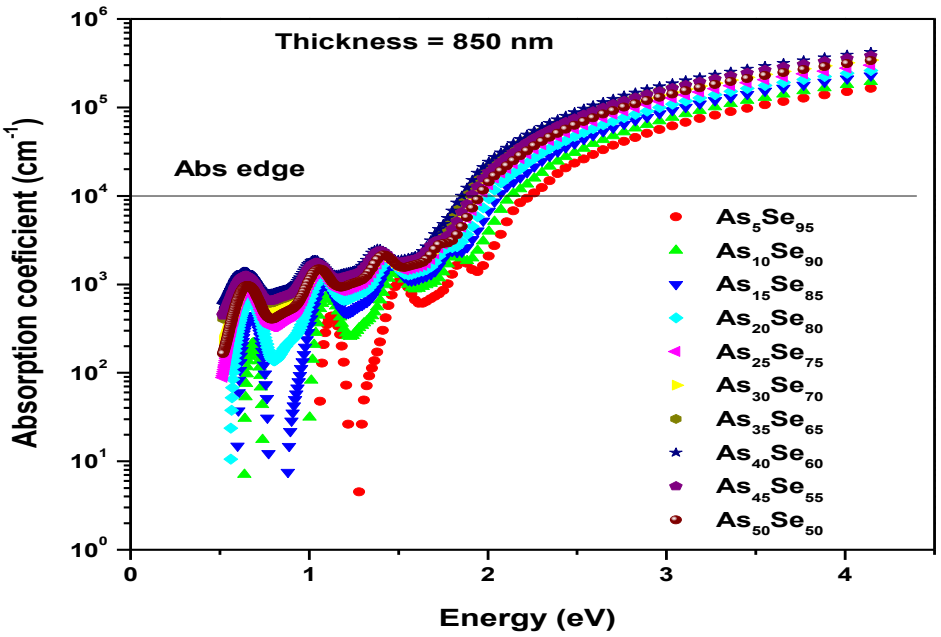

Figure 9 : Variation of (α) with the (hν) of As_xSe_{100-x} films

The spectral distribution of α is sectioned into two parts: High ($\alpha > 10^4$ cm^{-1}) and low absorption region ($\alpha < 10^4$ cm^{-1}). Urbach tail is usually located within the low absorption region [39], where α is described by:

$$\alpha(\nu) = \alpha_o \exp(h\nu / E_e) \quad (12)$$

Here h is the Plank constant, $h\upsilon$ is the photon energy, α_o is a constant, E_e is the width of the band tails of the localized states in the band gap. Therefore, we can determine the E_e values for As_xSe_{100-x} films by plotting ($\ln\alpha$) *vs.* E as shown in Figure 11, . The values of E_e increased with raising As content. This behavior is ascribed to the increased disorder within the system that participates in lowering E_g value with raising As content up to 40 at.% beyond this value, the band tail width (E_e) decreased.

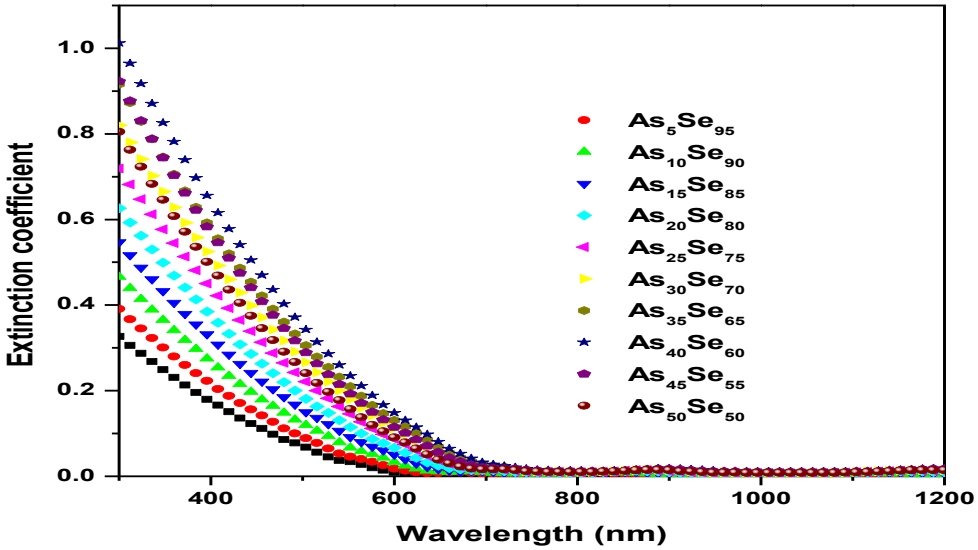

Figure 10: variation of k_{ex} with λ of the As_xSe_{100-x} thin films.

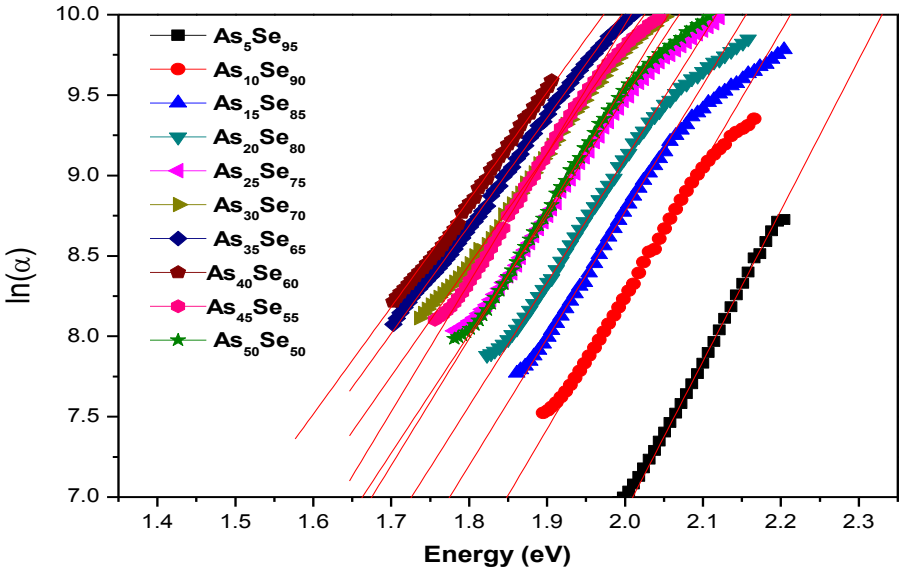

Figure 11 : Variation of ln(α) with the (hν) for As_xSe_{100-x} thin films

The second part of the spectral distribution absorption coefficient range starts at $\alpha \geq 10^4$ cm^{-1} and called the high absorption area. This region defines the optical band gap as it includes the optical transitions between extended states in both valence and conduction bands . The optical band gap was realized according to Tauc's relation [40]:

$$(\alpha h\nu) = B(h\nu - E_g)^r \quad (13)$$

where B is constant depends on the transition probability and E_g is the optical band gap of the specimen and r takes different values depending the involved type of transition within the film.

In order to decide the type of transition we have to test all the above values of r to find the relation which gives the best linear fit over the energy range above the absorption edge. The type of transition was found to be indirect allowed (r=2).

Plots of $(\alpha h\nu)^{0.5}$ vs. $h\nu$ for As_xSe_{100-x} films are shown in Figure 12. As we can see, E_g decreases with increasing As content up to 40% then increases for compositions containing As >40%. The reasons of the decrease of E_g for AsSe films (up to As=40 at. %) can be explained in relation to Mott and Davis approach and the structural theoretical calculations. According to Mott et al. [41], the degree of disorder and defects existing in the amorphous structure is defined by the localized states width close to the mobility edges. By adding arsenic, the As-Se bonds are created, that might deliver a more defects in the matrix. Such defects create localized states near the mobility edges. For films containing As≤40%, the As-Se bond concentration and subsequently the width of band tails (E_e) widens that causes the observed reduction in E_g. In addition, the basic matrix contains only the Se-Se bonds (selenium chains). By adding arsenic, the As-Se bonding is developed that leads to a shortage of homopolar Se–Se bonds. Thus, the numbers of extra bonds of Se-Se for each composition of the As_xSe_{100-x} system diminish as the As content raises, which is accordance to reduction in the E_g values . The decrease in energy gap values may be related to the reduction of extra homopolar bonds as the selenium has energy gap (1.95 eV) higher than the band gap of arsenic (1.1-1.2 eV) [42], i.e. the average bond strength of the composition weakens. Similar behavior was reported for the system $Se_{80-x}Te_{20}Bi_x$ [43]. Moreover, the decrease in E_g may be asserted by the reduction in the overall mean bond energy $\langle E \rangle$. The relation between band gap and $\langle E \rangle$is illustrated in Figure 13.

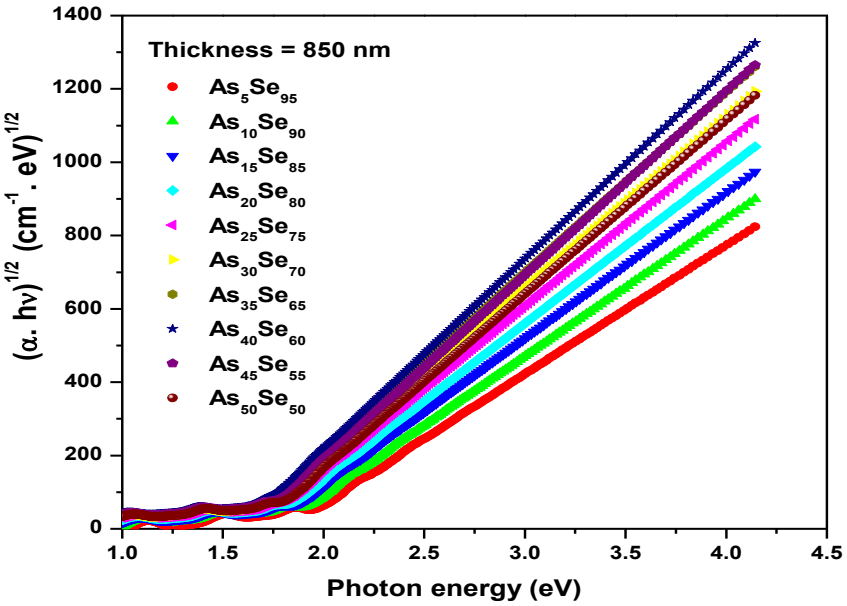

Figure 12 : Plots of $(\alpha h\nu)^{0.5}$ vs. $(h\upsilon)$ for As_xSe_{100-x} thin films

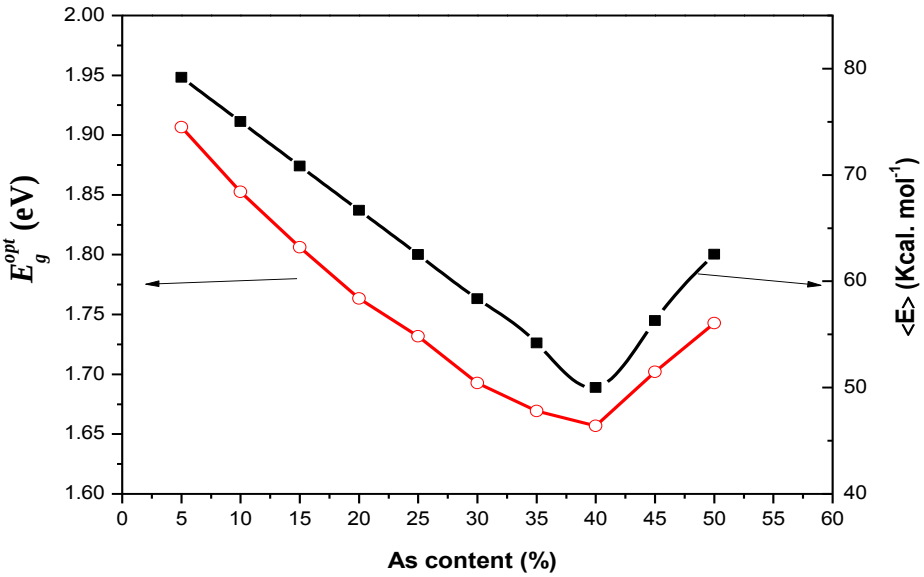

Figure 13: Variation of the E_g and $\langle E \rangle$ as a function of As content

On the other hand, the increase in optical gap values for compositions containing arsenic content higher than 40 at.% can be interpreted using average coordination number and fraction of floppy modes within the glassy system of AsSe. At As<40 at.%, system undergoes floppy state (where $\langle r \rangle < 2.4$), that implies high density of defects which in turn will affect the band gap. At $\langle r \rangle = 2.4$, the alloy is consisted of entirely cross-linked bonds (As-Se) without any excess of Se bonds in the alloy. More important, the system

changes from floppy state into rigid one. Thus, at $\langle r \rangle$ >2.4 we can expect increase in the band gap as the fraction of floppy modes decreases.

Table 3: optical parameters for As_xSe_{100-x} thin films

As (at. %)	E_g^{in} (eV)	E_e (eV)	E_o (eV)	E_d (eV)	S_o x10^{13} (m^{-2})	λ_o (nm)	ε_l	ε_∞	(N/m^*x10^{55}) $m^{-3}.Kg^{-1}$
٥	١.٩١	٠.١٠٦	٤.٠٢	١٥.٧٧	4.05	٣١١.١	٤.٩٥	٤.٩٢	2.85
١٠	١.٨٥	٠.١٢١	٣.٩٥	١٦.١٠	4.08	٣١٥.٥	٥.١٢	٥.٠٧	3.38
١٥	١.٨١	٠.١٢٦	٣.٩٠	١٦.٣٤	4.09	٣١٩.٨	٥.٢٥	٥.١٩	3.65
٢٠	١.٧٦	٠.١٣٠	٣.٨٧	١٦.٦٤	4.18	٣٢٠.٧	٥.٣٧	٥.٣٠	3.91
٢٥	١.٧٣	٠.١٣٥	٣.٨٦	١٧.٠٦	4.25	٣٢٢.٣	٥.٤٩	٥.٤٢	4.12
٣٠	١.٦٩	٠.١٤٤	٣.٨٢	١٧.١٢	4.26	٣٢٥.١	٥.٥٨	٥.٤٩	4.34
٣٥	١.٦٧	٠.١٤٩	٣.٨٠	١٧.٤١	4.35	٣٢٥.٧	٥.٦٨	٥.٥٨	4.53
٤٠	١.٦٦	٠.١٥٠	٣.٧٨	١٧.٦٨	4.36	٣٢٨.٠	٥.٧٨	٥.٦٨	4.60
٤٥	١.٧٠	٠.١٢٤	٣.٨٠	١٧.٥١	4.٣٥	٣٢٥.٤	٥.٧٠	٥.٦١	4.46
٥٠	١.٧٤	٠.١٢٦	٣.٨٢	١٧.٠١	4.31	٣٢٢.١	٥.٥٤	٥.٤٦	4.22

CONCLUSION

Glassy As_xSe_{100-x} alloys were prepared by using the melt quench method. The XRD analysis revealed non crystalline nature of the quenched glasses. The optical analyses of the semiconducting As_xSe_{100-x} films (x =5-50 at.%) have been done employing the data of T(λ) and R(λ). Through this study we adopted Swanepoel's method to determine the different optical parameters of AsSe films. The optical study of the As_xSe_{100-x} thin films reveals that *n* increases, while the indirect band gap changes from 1.91 to 1.77 eV with raising arsenic concentration upto 40 at.% and increase for films containing As >40 at.%. The behavior of the refractive index dispersion and its

dependence on composition of amorphous As_xSe_{100-x} thin films were studied using the single oscillator model.

REFERENCES

[1] B. J. Eggleton, B. Luther-Davies, K. Richardson, Chalcogenide Photonics, Nat. Photonics, 5 (2011) 141.

[2] A. Zakery, S. R. Elliott, Optical Properties and Applications of Chalcogenide Glasses: a Review, J. Non-Cryst. Solids, 330 (2003) 1.

[3] J. S. Sanghera, I. D. Aggarwal, Active and Passive Chalcogenide Glass Optical Fibers for IR Applications: a Review, J. Non-Cryst. Solids 256-257 (1999) 6.

[4] V. F. Kokorina, Glasses for Infrared Optics CRC Press, (2) Boca Raton, FL (USA) (1996).

[5] R. P. Wang, Amorphous Chalcogenides: Advances and Applications, Pan Stanford Publishing, Singapore, (2014).

[6] C. Quémard, F. Smektala, V. Couderc, Chalcogenide Glasses with High Non Linear Optical Properties for Telecommunications, J. Phys. Chem. Sol. (2001) 62 1435.

[7] J.S. Berkes, S.W. Ing, W.J. Hillegas, Photodecomposition of amorphous As_2Se_3 and As_2S_3, J. Appl. Phys. 42 (1971) 4908–4916

[8] J.P. DeNeufville, S.C. Moss, S.R. Ovshinsky, Photostructural transformations in amorphous As_2Se_3 and As_2S_3 films, J. Non-Cryst. Solids 13 (1973) 191.

[9] A. van Popta, R. Decorby, C. Haugen, T. Robinson, J. McMullin, Tonchev, S. Kasap, Photoinduced Refractive Index Change in As_2Se_3 by 633 nm Illumination. Opt. Express, 10 (2002) 639.

[10] W. Yuan, 2–10 Mm Mid-Infrared Supercontinuum Generation in As_2Se_3 Photonic Crystal Fiber, Laser Phys. Lett. 10 (2013) 095107.

[11] P. Toupin, L. Brilland, G. Renversez, J. Troles, All-Solid All-Chalcogenide Microstructured Optical Fiber, Opt. Express 21 (2013), 14643.

[12] N. Prasad, D. Furniss, H. L. Rowe, C. A. Miller, D. H. Gregory, A. B. Seddon, First Time Microwave Synthesis of As40Se60 Chalcogenide Glass., *J. Non-Cryst. Solids* (2010) *356* 2134.

[13] A.V. Kolobov, Photo-induced Metastability in Amorphous Semiconductors, Wiley-WCH, Weinheim, (2003) 23.

[14] J.C. Phillips, M. F. Thrope, Solid State Commun. 53 (1985) 699.

[15] J. C. Phillips, Constraint theory and stiffness percolation in network glasses. In: Thorpe M, Duxbury P M (eds.) Rigidity Theory and Applications. Kluwer, Dordrecht, The Netherlands, (1999) .

[16] L. Tichý, H. Tichá, Mater. Lett. 21 (1994) 313.

[17] J. C. Phillips, Rev. Mod. Phys. 49 (1970) 317.

[18] A. Dahshan , K. A. Aly, Philosophical Magazine, (2008)

[19] M.F. Thorpe, J. Non-Cryst. Solids 57(1983) 355.

[20] S.R. Ovshinsky, D. Adler, J. Contemp. Phys. 19 (1978) 109.

[21] J. Bicerano, S. R. Ovshinsky, J. Non-Cryst. Solid, 74 (1985)75

[22] L. Pauling, *The Nature of the Chemical Bond* ,Cornell University Press Ithaca, NY, (1960)

[23] L. Tichý, A. Tříska, H. Ticha, M. Frumar, J. Klikorka, Solid State Commun. 41 (1982) 751.

[24] S. A. Fayek, M. R. Balboul, K. H. Marzouk, thin soild films, 515 (2007) 7281-7285.

[25] R. Sathyamoorthy, J. Dheepa, J. Phys. Chem. Sloids. 68 (2007) 111-117.

[26] S.A. Fayek, Infrared Phys.Technol. 46 (2005) 193–198

[27] H.A. Abd El Ghani, M.M. Abd El Rahim, M.M. Wakkad, A. Abo Sehli, N. Assraan, Physica B 381 (2006) 156–163

[28] R. Swanepoel, "Determination of the thickness and optical constants of amorphous silicon", J. Phy. E: Sci Instrm., 16 (1983) 1214-1222.

[29] E.R. Shaaban, N. Afify, A. El-Taher, J. Alloys Compd. 482 (2009) 400.

[30] M. Emam-Ismail, E.R. Shaaban, M. El-Hagary, I. Shaltout, Philos. Mag. B90 (2010) 3499.

[31] J.N. Zemel, J. D. Jensen, R. B. Schoolar, Phys. Rev. A 140 (1965) 330.

[32] T. S. Moss, G. J. Burrell, E. Ellis, Semiconductor Opto-Electronics, Butterworths, London, Englad (1973).

[33] H. Wemple, M. Di Domininco, J. Appl. Phys., 40 (1969) 735.

[34] S. H. Wemple, M. Di Domininco, Phys. Rev., 3 (1971) 1338.

[35] A. K. Wolaton, T. S. Moss, Proc. R. Soc. 81 (1963) 5091.

[36] M. Emam-Ismail, M. El-Hagary, E.R. Shaaban, A.M. Al-Hedeib, J. Alloys Compd. 532 (2012) 16–24

[37] T. S. Moss, optical properties of semiconductors , Butterworths, London, (1959).

[38] G.A.N. Connell, A.J. Lewis, Phys. Status Solidi, B Basic Res. 60 (1973) 291.

[39] R. Urbach, Phys. Rev., 92 (1953) 1324.

[40] J.Tauc, R. Grigorovici and A.Vancu, Phys. Stat. Sol., 15 (1966) 627.

[41] N. F. Mott and E. A. Davis, "Electronic processes in Non-crystalline Materials" 2nd ed., Oxford Univ. Press (1979).

[42] W. J. Hillegas and J. H. Neyhart, J. Appl. Phys. 49 (1978) 838

[43] E.R. Shaaban, Yasser A.M. Ismail, H. Shokry Hassan, J. Non-Cryst. Solids 376 (2013) 61–67